Fracture toughness and temperature dependence of Young's modulus of a sintered albite glass

Marcelo Dal Bó [a*], Vicente Cantavella [b], Enrique Sánchez [b], Dachamir Hotza [a], Francisco A. Gilabert [b]
[a] *Graduate Program in Materials Science and Engineering (PGMAT), Department of Chemical Engineering (EQA), Federal University of Santa Catarina (UFSC), 88040-900 Florianópolis, SC, Brazil*
[b] *Institute of Ceramic Technology (ITC), Universidad Jaume I (UJI), Campus Riu Sec, 12006 Castellón, Spain*

* Corresponding author: Tel.: +55 48 3465 4882; fax: +55 48 3721 7615
E-mail address: marcelodalbo@hotmail.com (Dal Bó, M.)

Abstract: Albite glass is an important component in many ceramic compositions, often used as liquid phase during the sintering process. Nevertheless, in spite of its almost ubiquous presence in the final microstructure of these compositions, some properties such as Young's modulus or fracture toughness have not been extensively studied in literature. This paper presents an experimental study on a sintered albite glass obtained from sodium feldspar powder. The microstructure of the resultant amorphous solid was analyzed via scanning electron microscopy and x-ray diffraction. . Fracture toughness was determined at room temperature from the critical stress intensity factor (K_{IC}) with a three point bending single-edge notched test (SENB). Young's modulus and coefficient of thermal expansion (*CTE*) were measured as a function of the temperature. A value of *CTE* of 6.6×10^{-6} ºC^{-1} within the temperature range 300-500ºC was found. The Young's modulus values of the albite glass were within the range from 63.6 to 65.2 MPa. SENB tests revealed a fracture toughness of $K_{IC} = 0.78 \pm 0.06$ MPa·m$^{1/2}$, which is similar value to those found for borosilicate and soda-lime glasses.

Keywords: albite glass, sodium feldspar, fracture toughness, temperature-dependence, Young's modulus, thermal expansion.

1. Introduction

The understanding of the structure of many silicates melts goes necessarily through a comprehensive analysis of the relationship between microstructural features and thermomechanical properties of the melts. Many studies addressed to understand these relationships have been carried out using similar melts systems. In those works it has been hypothesized that the features of the structure of these materials in the molten state are maintained after they have reached the glassy state [1]. This hypothesis that poses the similarity between the silicate melts and the glass state was confirmed by Sweet et al. using infrared rays on compositions in the system $Na_2O{\cdot}SiO_2$ [2]. A similar conclusion was reached from studies with melts and glasses of the systems $Na_2O{\cdot}Al_2O_3{\cdot}SiO_2$ and GeO_2, in which Raman spectroscopy was used [3].

Furthermore, this structural parallelism between the melts and their glasses could be verified analyzing the X-ray radial distribution functions obtained from a liquid of $NaAlSi_3O_8$ composition that was supercooled [4]. Moreover, Domine et al. [5] carried out a study with an extensive frequency range of the infrared reflectance spectra, concluding that is reasonable to extrapolate the knowledge of silicate glasses to silicate melts. As a summary, experiments on quenched glasses are much easier than similar experiments on melts but they require the assumption that the structure of the quenched glass reflects the structure of the melt.

Silicate glasses constitute the base for a long tradition, manufacturing industry, i.e., glass industry. Therefore, the correspondence between the glass properties and silicate melt performance in these homogeneous systems has been extensively addressed. However, silicate glasses also occur as a glassy matrix of many of the products commonly named traditional ceramics together with other crystalline phases such as quartz, feldspar, and alumina. Thus, the preparation and characterization of model glasses resembling these glassy matrixes represents an inevitable and necessary aspect when designing these ceramics compositions.

Albite glass is one of the most common glassy matrixes. This glass is originated from sodium feldspar, a mineral widely used in the production of porcelain stoneware [6-8], ceramic glazes [9], conventional glasses [10], dental ceramics [11, 12], abrasive tools [13], compositions produced by recycling waste [14-17] and metal matrix composites [18, 19]. During the manufacture of those materials, the sintering process causes the albite crystals to melt at 1100ºC, transforming them into albite glass [20].

Thermal conditions along the process configure the final mechanical properties of the material. Therefore, in the same manner in which it is essential to know the composition and the proportion of the phases, it is also crucial to have each of them well characterized within the range of process temperature. The melting of crystals dynamically modifies their behaviour during thermal cycle. This structural change alters, in general, the

anisotropy, thus modifying the efficiency with which the thermal and mechanical loads are transmitted through its microstructure [21].

Thermal and rheological properties of albite glass such as diffusivity, coefficient of thermal expansion (*CTE*), heat capacity and viscosity have already been determined [10, 22-24]. On the other hand, some geological features of albite as weathering [25-27], dissolution kinetics in aqueous and/or acid solutions[28-30], crystallization kinetics [31], leaching [32] also have been studied. Nevertheless, there are no specific studies dealing with fracture toughness (K_{IC}) as well as temperature dependence of the Young's modulus (E) for albite glass.

During sintering, the microstructure of ceramic materials is vulnerable to microscopic stresses during cooling, due to the thermal expansion mismatch between the vitreous and crystalline phases. If this mismatch is intense enough, cracks can be microscopically detected [33]. From the macroscopic side, this damage considerably affects the mechanical performance [34-37]. To control and minimize this damage it is essential to know how E and *CTE* evolve as a function of temperature for each constituent phase. This knowledge allows carrying out predictions using computer simulations, where specific properties of each constituent material must be known [38-41].

In this study it is assumed that the main characteristics of the structure remain constant during the molten state towards the final glassy state [1-5, 42], so that reliable measurements were carried out for some mechanical and thermal properties, at room and higher temperatures.

This paper is organized as follows. In section 2 the experimental procedure is presented, including the preparation of specimens of albite glass and the instrumentation needed to characterize them. Section 3 presents the microstructural analysis of the specimens, as well as the results of Young's modulus, fracture toughness and coefficient of thermal expansion. In section 4 those results are discussed and, finally, the most relevant aspects found for the synthetic albite glass are highlighted.

2. Experimental

2.1- Specimen preparation

To synthesize albite glass, a sodium feldspar powder (Mario Pilato, Spain) was used, whose composition is presented in Table 1. After melting, the high percentage of sodium oxide, in comparison with

other oxides like calcium and potassium, ensures that the obtained material can be classified as albite glass. Sodium feldspar was wet milled using alumina balls at 260 rpm during 30 min, resulting in a particle size of 6.3 μm (D_{50}), as shown in Fig. 1. The milled powder was then melted in an electric furnace (Carbolite model BLF 1800). The heating rate was initially 25ºC/min up to 500ºC and then decreased to 10ºC/min up to a temperature of 1650ºC, which was maintained during 3.5 h. With the aim of obtaining an amorphous state, the material resulting from melting was subjected to a quenching process in air to reach room temperature. The albite glass was crushed and dry milled during 15 min at 260 rpm. The powder generated was granulated with 8 wt.% of an aqueous solution with a concentration of 5 wt.% PVA (Polyvinyl alcohol, Mowiol 4-88, molecular weight 31000 g/mol, Sigma-Aldrich). With this mixture, ten specimens were uniaxially pressed at 35 MPa, whose final dimensions were 7.0×1.7×0.6 cm. After drying during 3 h, the specimens were fired in an electric furnace (Pirometrol R-series). Samples were heated at 210ºC/min until reaching 500ºC; the heating rate was then decreased to 25ºC/min up to 1200ºC. The samples were maintained at this temperature for 6 min. The furnace was then turned off and samples were cooled down inside the kiln until reaches room temperature. Finally, the bulk density was measured by Archimedes' principle. The porosity was then calculated from picnometric [10] and bulk density.

Table 1 Chemical composition of sodium feldspar (albite, $Na_2O{\cdot}Al_2O_3{\cdot}6SiO_2$).

Oxide	Composition studied (wt.%)	Theoretical composition (wt.%)
SiO_2	69.90	68.74
Al_2O_3	18.70	19.44
Na_2O	10.00	11.82
K_2O	0.30	---
CaO	0.50	---
MgO	0.10	---
Fe_2O_3	0.06	---
Loss on ignition	0.30	---

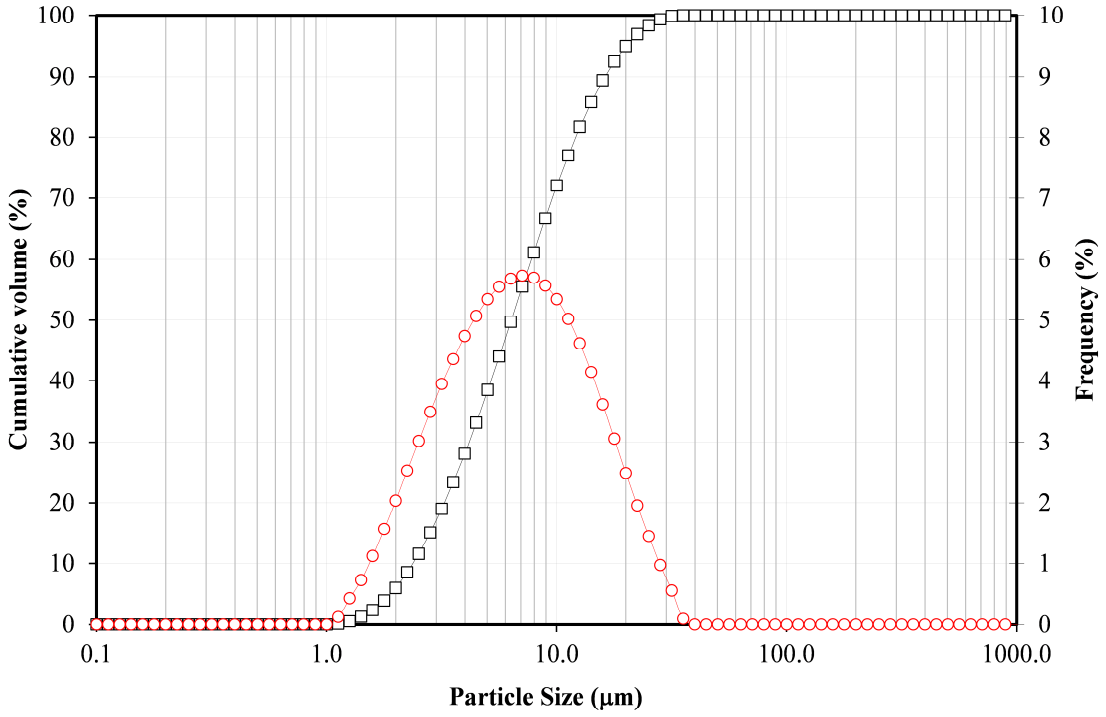

Fig. 1 Particle size distribution of sodium feldspar after milling.

2.2- Microstructural characterization

To identify potential crystalline phases, the analyzes were performed on the surface of the sample via X-ray diffraction test. The selected instrument (D8 Advance, Bruker, Germany) used Cu $K_{\alpha 1,2}$ (1.5406 Å) radiation, with a goniometer radius of 250 mm. The data were collected on a diffractometer with Bragg-Brentano geometry (θ/θ), between 5 and 90º (2θ), with a step size of 0.015º to 1s per step. The diffractometer optics consisted of a primary system of Soller slits and a fixed aperture of 0.5 mm. A rapid solid-state detector (Vantec, Bruker, Germany) fitted with a system of Soller slits and nickel filter was used. The X-ray tube operated at 40 kV and 45 mA.

The glass microstructure was studied using a scanning electron microscope (FEI Quanta 200 ESEM FEG), coupled with a chemical analysis sensor (EDAX) to obtain an auxiliary chemical analysis from the observed image. To perform this analysis, the samples were cut in cross section and embedded in a block made of epoxy resin. The exposed surface was polished using fine abrasives progressively until finishing with 1 µm diamond. Subsequently, the specimens were washed with distilled water in an ultrasonic bath. Once clean and

dried, they were inspected and photographed with the backscattered electron signal of the scanning electron microscope of field emission. The backscattered electron signal provides information on composition. The observation was performed using accelerated electrons with different potentials (10, 15 and 20 kV) in such a way that the lower the acceleration potential of the electrons, the weaker the signal. Additionally, the samples were also analyzed using a microanalysis equipment energy dispersive X-ray (EDX) attached to the microscope.

2.3- Thermal and mechanical characterization

The coefficient of thermal expansion (*CTE*) and the glass transition temperature (T_g) were determined by a dilatometer (Adamel-Lhomargy, model DI-24), calibrated with a pattern of sapphire. The thermal cycle used was a warm up of 5ºC/min to the maximum temperature of 1000ºC.

The measurement of Young's modulus (*E*) was carried out using the impulse excitation technique [43-45]. This technique is a procedure that consists in generating a flexural vibration by means of a non-destructive mechanical impulse. This frequency depends on two magnitudes: the mass of the specimen and its stiffness. The latest factor can be determined by its dimensions, specific shape and the elastic modulus of the constituent material. An apparatus (Grindosonic, model MK5I) was especially conceived to measure the natural frequency of vibration along a programmable thermal cycle. Once the vibration sequence is captured, the signal is subjected to a time-domain analysis. In this way, the fundamental frequency of the object can be accurately detected as a function of the temperature. The cycle consisted of heating up to 700ºC at a constant rate of 6.6ºC/min. Once this temperature was reached, the measuring device was turned off and the specimen was cooled within the chamber until reaching the room temperature.

For the case concerning this work prismatic specimens were used. With this configuration, the relationship between the frequency of the first vibrational mode and the elastic modulus is given by the following expression [43-45].

$$E = \rho\left(f\frac{L}{e} \right)^2 A \tag{1}$$

where f is the natural frequency of the object, ρ is the material density, L and e are length and thickness of the specimen, respectively, and A is a correction factor given by

$$A = 0.946\left(1 + 6.585\left(\frac{e}{L}\right)^2\right) \tag{2}$$

This correction factor involves that dimensions of the specimen must satisfy $L/e > 10$ [43-45].

Fracture toughness was measured only at room temperature. The stress intensity factor associated to fracture mode-I, K_{IC}, has been obtained according to ASTM C1421-10 [46] using a configuration of single-edge notched bending (SENB). An initial precrack with 0.5 mm width was made using a high precision circular saw provided with a diamond wheel. The initial incision was then inspected under the optical microscope to determine the real cut depth. A detail of the length measurement of the initial crack is depicted in Fig. 2.

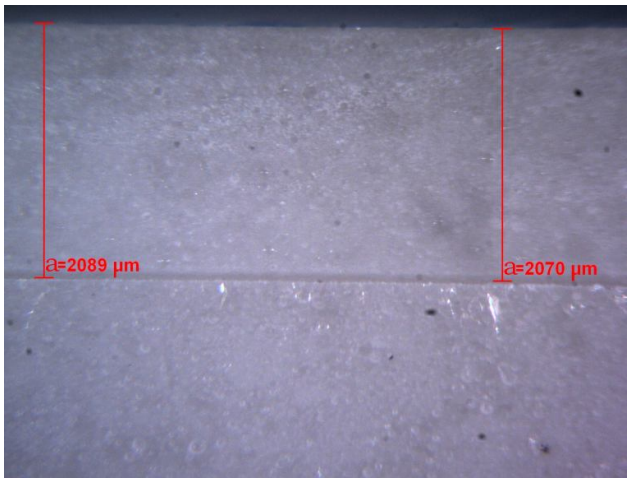

Fig. 2 Optical micrograph of a cross sectional area of the notched region and measurement of the precrack length.

The specimen was arranged in a three-point bending bridge, and mounted on a universal testing machine (Instron, model 6027), at a strain rate of 1 mm/min. The Griffith's criterion [47] is an adequate procedure to determine the fracture toughness in brittle materials. This criterion establishes a simple relationship between the initial crack length and the fracture toughness given by [48]

$$K_{IC} = Y\sigma_R\sqrt{a} \tag{3}$$

where a is the initial crack length, σ_R is the maximum stress at fracture measured during the experimental realization and Y is a factor that depends on the specimen geometry. A total of eight specimens were tested.

3. Results

3.1- Microstructural characterization

As set out above experiments on quenched glasses are much easier than similar experiments on melts but require the assumption that the structure of the quenched glass reflects the structure of the melt, for which there is some evidence in silicate systems [42]. Based on this evidence, the XRD can be used to analysis the amorphous phase of albite.

Fig. 3 shows the results of XRD analysis of albite glass. This result confirms the absence of crystalline phases, thus ensuring the amorphous character of the produced glass. According to Navarro [10], the theoretical bulk density of albite glass is 2418 kg/m . In the present work, measurements revealed a value of 2285 ± 3 kg/m , which corresponds to a porosity of ca. 5%. It is worth mentioning that Taylor et al. found a value of 2382 kg/m [42], which is also close to the result found here. These data mean that the degree of homogeneity of this albite glass is fairly good, what moreover is clearly reflected by the micrographs from Fig. 4, where the typical aspect of the final microstructure obtained from one of our specimens is shown. From a mechanical point of view, this low percent of porosity has a negligible impact on the mechanical performance, in particular on the Young's modulus [49, 50].

Table 2 shows the semi-quantitative chemical analysis of glass by EDX, which is very similar to the theoretical composition of albite glass ($Na_2O{\cdot}Al_2O_3{\cdot}6SiO_2$).

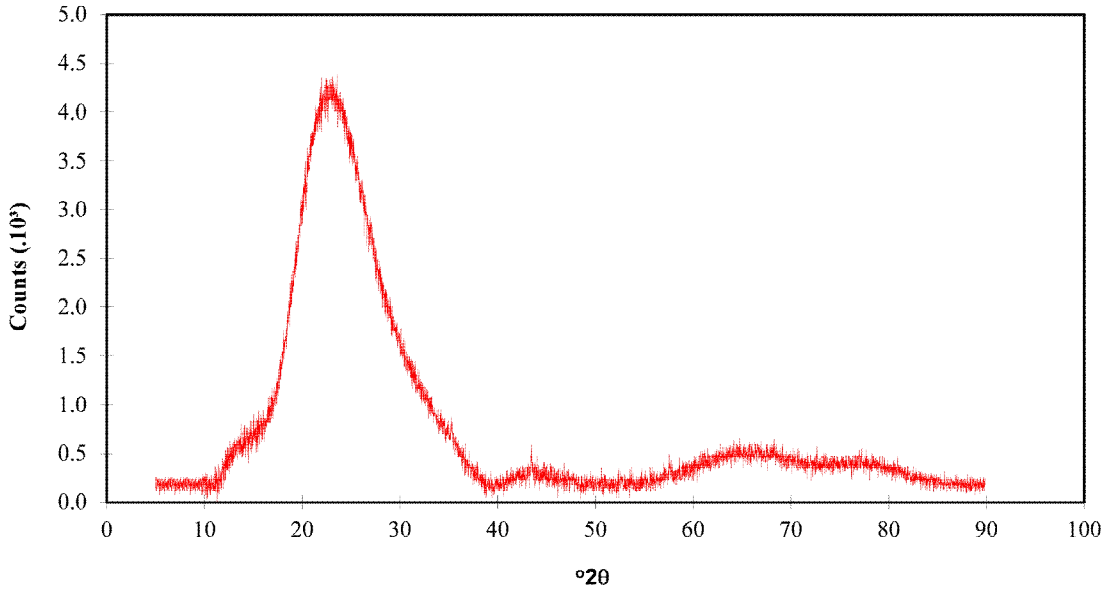

Fig. 3 XRD of albite glass.

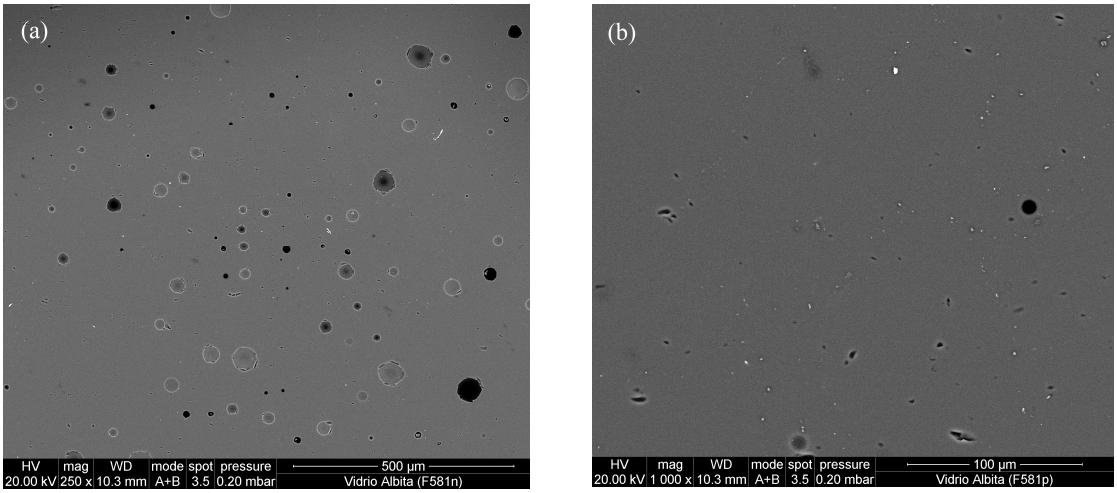

Fig. 4 SEM micrographs of albite glass at different magnifications: (a) 250×; (b) 1000×.

Table 2 Experimental vs. theoretical chemical composition ($Na_2O{\cdot}Al_2O_3{\cdot}6SiO_2$).

Oxides	**Experimental (wt.%)**	**Theoretical (wt.%)**
SiO_2	72.05	68.74
Al_2O_3	18.81	19.44
Na_2O	9.14	11.82

Sum	100.00	100.00

3.2- Thermal and mechanical characterization

In Fig. 5, the temperature dependence of the coefficient of thermal expansion is shown. As it can be seen, the glass of albite reveals a nearly linear behaviour up to ~750ºC, from which the vitreous transition begins to take place. Concerning the aforementioned linearity, the difference between the two values of *CTE* within the two most commonly used temperature ranges resulted to be poorly significant, as it can be appreciated in Table 3. The glass transition temperature measured by the dilatometer was 819ºC, which is consistent with data available in the literature [10, 51].

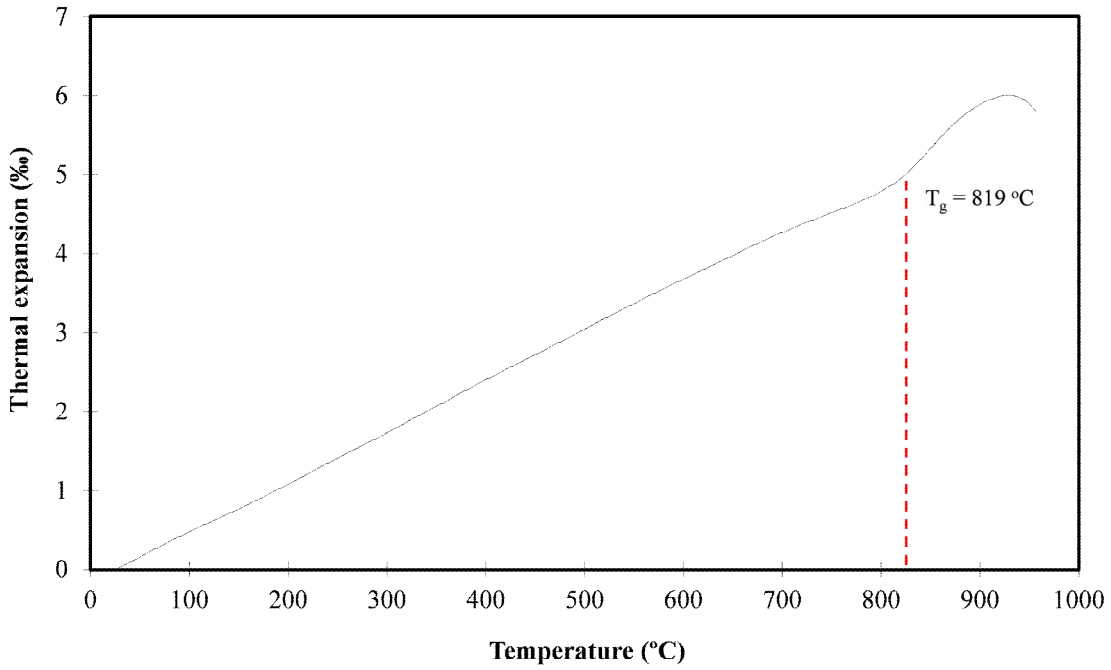

Fig. 5 Coefficient of thermal expansion and transition temperature of albite glass.

Table 3 Coefficient of thermal expansion of albite glass.

CTE	Value ($ºC^{-1}$)
$\alpha_{50\text{-}300}$	$6.3 \cdot 10^{-6}$
$\alpha_{300\text{-}500}$	$6.6 \cdot 10^{-6}$
$\alpha_{500\text{-}650}$	$6.2 \cdot 10^{-6}$

Fig. 6 shows the elastic modulus of albite glass as a function of the temperature. During the first records of the thermal cycle, with the temperature increasing, a slight drop of stiffness of 1.5 MPa was detected within the range between 20 and 120ºC. From this point, a clear change of trend was produced, in which the elastic modulus started to increase progressively. Once the temperature reached the maximum prescribed value of 700ºC, the elastic modulus recovered the lost stiffness, reaching the original value at room temperature. This variation of elasticity corresponds to 2.2% of the elastic constant at room temperature. On the other hand, regarding the elastic modulus at room temperature, after carrying out a statistical analysis considering all specimens, 50% of the values were within the range from 64.2 to 65.7 MPa.

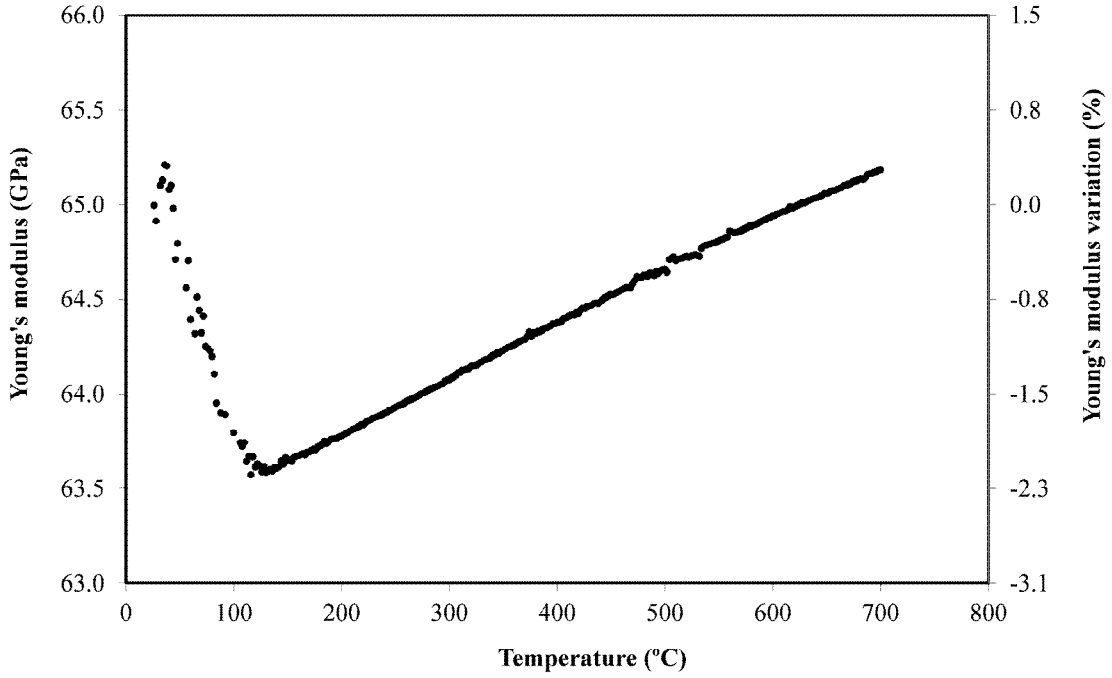

Fig. 6 Temperature influence on the elastic modulus of albite glass.

The results of fracture toughness are shown in Table 4. The second column in this table shows the initial crack length measured with the aid of the optical microscope. The measured load to fracture of each specimen is listed in the third column. The last column is the stress intensity factor obtained using Eq. 3. These results show that statistically 50% of the data are within the range from 0.72 to 0.82 MPa·m$^{1/2}$. This interval would represent the inter-quartile range in a box plot. It is worth mentioning that, in the obtained distribution, the mean value is $K_{IC} = 0.78 \pm 0.06$ MPa·m$^{1/2}$. This result confirms that the fracture toughness of the albite glass

is very close to the fracture toughness of other types of glasses, such as soda-lime glass (K_{IC} ~ 0.75 MPa·m$^{1/2}$) [52].

Table 4 Albite glass fracture toughness: specimen tag, mean precrack length, maximum applied load, stress at rupture and fracture toughness.

Sample	a (μm)	*Load* (N)	σ_R (MPa)	K_{IC} (MPa.m$^{1/2}$)
1	2454.5	134.10	8.56	0.79
2	2079.5	91.41	9.03	0.78
3	2874.0	55.36	5.91	0.70
4	2287.0	63.39	7.16	0.69
5	2499.0	61.33	7.07	0.74
6	2217.0	80.85	8.96	0.84
7	2408.0	78.55	8.80	0.88
8	1813.8	88.32	9.89	0.80

As a reference, typical porcelainware compositions and many dental composites usually exhibit fracture toughness between 1.5 and 5 MPa·m$^{1/2}$ [53-58].

4. Discussion

The microstructural characterization showed that the albite glass presented high purity and low porosity. According to the mechanical characterization of albite glass, Fig. 6, the elastic modulus at room temperature was 65 GPa, which is similar to the elastic modulus of soda-lime glass (73 GPa) [59]. This result also shows that the *E* value of albite glass had a very weak dependence on the temperature within the range from 20 to 700ºC. In addition, this process was completely reversible within this range. According to Soga [60], the elastic modulus in glasses depend on the chemical composition, microstructure, temperature and packing state. In particular, it was shown that the soda-lime glasses exhibit a linear behaviour from room temperature up to 540ºC (T_g), which was not found for amorphous albite.

The fracture toughness obtained for albite glass represents the typical value of homogeneous and brittle materials such as glasses. This value is coherent with those results found for borosilicate and soda-lime glasses [10, 52, 61, 62], which are around 0.7 MPa·m$^{1/2}$. In general, the fracture toughness of glasses is lower than that

of polycrystalline ceramics and ceramic composites [60]. These latest usually exhibit higher fracture energy since they may count with micromechanisms that hinder the crack propagation (microcrack toughening, bridging, process-zone toughening or transformation toughening, among others). In an amorphous structure those mechanisms are typically absent, what explains the obtained value.

The measurements of the fracture toughness and the elastic modulus of albite glass represent an interesting contribution to the knowledge of the mechanical properties of this type of glass. This knowledge is very useful to predict the fracture resistance of many ceramic compositions. Often these materials make use of albite glass, or quite similar, as liquid phase for driving the formation of the microstructure. The current experimental measurements can be used as input data in many theoretical predictions where ceramic composites made of crystalline particles embedded in a vitreous matrix are involved [63-65].

5. Conclusions

In this paper albite glass was obtained and characterized. Coefficient of thermal expansion, glass transition temperature, Young's modulus and fracture toughness were measured.

The chemical analysis confirmed an albite glass with an acceptable purity. Likewise, the obtained material microstructure has been also analyzed by scanning electron microscopy, revealing a low residual porosity. Regarding albite properties, the coefficient of thermal expansion presented a nearly linear dependence on the temperature, up to the glass transition at 819ºC. The elastic modulus was practically unchanged by the effect of temperature in the range between 20ºC and 700ºC, presenting values within the range from 63.6 to 65.2 MPa. The albite glass fracture toughness, 0.78 $MPa \cdot m^{1/2}$, is within the range obtained for typical glass compositions, such as borosilicate or soda lime glasses.

Acknowledgements: This work was financially supported by the Spanish Ministry of Science and Innovation, within the National Program for Fundamental Research Projects (BIA2009-10692), and by the Brazilian Program CAPES-DGU (Coordenação de Aperfeiçoamento de Pessoal de Nível Superior, BEX 6505/10-4).

References

[1] B.O. Mysen, The structure of silicate melts, Annual Review of Earth and Planetary Sciences, 11 (1983) 75-97.

[2] J.R. Sweet, W.B. White, Study of sodium silicate glasses and liquids by infrared reflectance spectroscopy, Physics and Chemistry of Glasses, 10 (1969) 246-251.

[3] F.A. Seifert, B.O. Mysen, D. Virgo, Structural similarity of glasses and melts relevant to petrological processes, Geochimica et Cosmochimica Acta, 45 (1981) 1879-1884.

[4] M. Taylor, G.E. Brown Jr, P.M. Fenn, Structure of mineral glasses—III. $NaAlSi_3O_8$ supercooled liquid at 805°C and the effects of thermal history, Geochimica et Cosmochimica Acta, 44 (1980) 109-117.

[5] F. Domine, B. Piriou, Study of sodium silicate melt and glass by infrared reflectance spectroscopy, Journal of Non-Crystalline Solids, 55 (1983) 125-130.

[6] S.K. Das, K. Dana, Differences in densification behaviour of K- and Na-feldspar-containing porcelain bodies, Thermochimica Acta, 406 (2003) 199-206.

[7] S.L. Correia, K.A.S. Curto, D. Hotza, A.M. Segadães, Using statistical techniques to model the flexural strength of dried triaxial ceramic bodies, J Eur Ceram Soc, 24 (2004) 2813-2818.

[8] C. Zanelli, M. Raimondo, G. Guarini, M. Dondi, The vitreous phase of porcelain stoneware: Composition, evolution during sintering and physical properties, Journal of Non-Crystalline Solids, 357 (2011) 3251-3260.

[9] R. Casasola, J. Rincón, M. Romero, Glass–ceramic glazes for ceramic tiles: a review, Journal of Materials Science, 47 (2012) 553-582.

[10] J.M.F. Navarro, El Vidrio, CSIC, Madrid, 2003.

[11] X.-F. Song, L. Yin, Y.-G. Han, H. Wang, Micro-fine finishing of a feldspar porcelain for dental prostheses, Medical Engineering & Physics, 30 (2008) 856-864.

[12] C.C. Gonzaga, P.F. Cesar, W.G. Miranda Jr, H.N. Yoshimura, Slow crack growth and reliability of dental ceramics, Dental Materials, 27 (2011) 394-406.

[13] M.J. Jackson, B. Mills, Microscale wear of vitrified abrasive materials, Journal of Materials Science, 39 (2004) 2131-2143.

[14] B. Karasu, M. Çakı, Y.G. Yeşilbaş, The effect of albite wastes on glaze properties and microstructure of soft porcelain zinc crystal glazes, J Eur Ceram Soc, 21 (2001) 1131-1138.

[15] M.S. Hernández-Crespo, J.M. Rincón, New porcelainized stoneware materials obtained by recycling of MSW incinerator fly ashes and granite sawing residues, Ceramics International, 27 (2001) 713-720.

[16] R. Rawlings, J. Wu, A. Boccaccini, Glass-ceramics: Their production from wastes—A Review, Journal of Materials Science, 41 (2006) 733-761.

[17] A.P. Luz, S. Ribeiro, Use of glass waste as a raw material in porcelain stoneware tile mixtures, Ceramics International, 33 (2007) 761-765.

[18] S. Sharma, Effect of aging on oxidation behavior of aluminum-albite composites at high temperatures, Journal of Materials Engineering and Performance, 9 (2000) 344-349.

[19] K.H.W. Seah, M. Krishna, V.T. Vijayalakshmi, J. Uchil, Effects of temperature and reinforcement content on corrosion characteristics of LM13/albite composites, Corrosion Science, 44 (2002) 761-772.

[20] J.P. Greenwood, P.C. Hess, Congruent melting kinetics of albite: Theory and experiment, Journal of Geophysical Research, 103 (1998) 29815-29828.

[21] P.R. Okamoto, N.Q. Lam, L.E. Rehn, Physics of Crystal-to-Glass Transformations, in: E. Henry, S. Frans (Eds.) Solid State Physics, Academic Press, 1999, pp. 1-135.

[22] C.M. Scarfe, D.J. Cronin, Viscosity-temperature Relationships of Metls at 1atm in the System Diopside-Albite, American Mineralogist, 71 (1986) 767-771.

[23] A. Hofmeister, A. Whittington, M. Pertermann, Transport Properties of High Albite Crystals, Near-endmember Feldspar and Pyroxene Glasses, and their Melts to High Temperature, Contributions to Mineralogy and Petrology, 158 (2009) 381-400.

[24] D. Cranmer, D.R. Uhlmann, Viscosity of liquid albite, a network material, Journal of Non-Crystalline Solids, 45 (1981) 283-288.

[25] G.R. Holdren Jr, R.A. Berner, Mechanism of feldspar weathering—I. Experimental studies, Geochimica et Cosmochimica Acta, 43 (1979) 1161-1171.

[26] R.A. Berner, G.R. Holdren Jr, Mechanism of feldspar weathering—II. Observations of feldspars from soils, Geochimica et Cosmochimica Acta, 43 (1979) 1173-1186.

[27] L. Chou, R. Wollast, Study of the weathering of albite at room temperature and pressure with a fluidized bed reactor, Geochimica et Cosmochimica Acta, 48 (1984) 2205-2217.

[28] Y. Tsuzuki, S. Kadota, I. Takashima, Dissolution process of albite and albite glass in acid solutions at 47°C, Chemical Geology, 49 (1985) 127-140.

[29] J.P. Hamilton, C.G. Pantano, S.L. Brantley, Dissolution of albite glass and crystal, Geochimica et Cosmochimica Acta, 64 (2000) 2603-2615.

[30] K.G. Knauss, T.J. Wolery, Dependence of albite dissolution kinetics on ph and time at 25°c and 70°c, Geochimica et Cosmochimica Acta, 50 (1986) 2481-2497.

[31] A. Karamanov, M. Pelino, Sinter-crystallization in the diopside–albite system: Part II. Kinetics of crystallization and sintering, J Eur Ceram Soc, 26 (2006) 2519-2526.

[32] Y. Chen, S.L. Brantley, E.S. Ilton, X-ray photoelectron spectroscopic measurement of the temperature dependence of leaching of cations from the albite surface, Chemical Geology, 163 (2000) 115-128.

[33] A. De Noni Jr., D. Hotza, V. Cantavella, E.S. Vilches, Influence of Macroscopic Residual Stresses on the Mechanical Behavior and Microstructure of Porcelain Tile, J Eur Ceram Soc, 28 (2008) 2463-2469.

[34] B. Budiansky, R.J.O. Connell, Elastic Moduli of a Cracked Solid, Int. J. Solids Structures, 12 (1976) 81-97.

[35] L. Shen, S. Yi, Approximate Evaluation for Effective Elastic Moduli of Cracked Solids, International Journal of Fracture, 106 (2000) 15-20.

[36] L. Shen, J. Li, A numerical simulation for effective elastic moduli of plates with various distributions and sizes of cracks, International Journal of Solids and Structures, 41 (2004) 7471-7492.

[37] A. De Noni Jr., D. Hotza, V. Cantavella, E.S. Vilches, Effect of Quartz Particle Size on the Mechanical Behaviour of Porcelain Tile Subjected to Different Cooling Rates, J Eur Ceram Soc, 29 (2009) 1039-1046.

[38] V. Cannillo, A. Corradi, C. Leonelli, A.R. Boccaccini, A simple approach for determining the in situ fracture toughness of ceramic platelets used in composite materials by numerical simulations, Journal of Materials Science Letters, 20 (2001) 1889-1891.

[39] V. Cannillo, C. Leonelli, T. Manfredini, M. Montorsi, P. Veronesi, E.J. Minay, A.R. Boccaccini, Mechanical performance and fracture behaviour of glass–matrix composites reinforced with molybdenum particles, Composites Science and Technology, 65 (2005) 1276-1283.

[40] A.P.N.d. Oliveira, E.S. Vilches, V.C. Soler, F.A.G. Villegas, Relationship between Young's modulus and temperature in porcelain tiles, J Eur Ceram Soc, 32 (2012) 2853-2858.

[41] F.A. Gilabert, V. Cantavella, E. Sánchez, G. Mallol, Modelling fracture process in ceramic materials using the Material Point Method, EPL (Europhysics Letters), 96 (2011) 24002.

[42] M. Taylor, G.E. Brown Jr, Structure of mineral glasses - I. The feldspar glasses $NaAlSi_3O_8$, $KAlSi_3O_8$, $CaAl_2Si_2O_8$, Geochimica et Cosmochimica Acta, 43 (1979) 61-75.

[43] W. Lemmens, Dynamic Measurements in Materials, American Society for Testing and Materials, Philadelphia, 1990.

[44] M. Charles S, Elastic Modulus Versus Bond Length in Lanthanum Chromite Ceramics, J Eur Ceram Soc, 18 (1998) 353-358.

[45] ASTM, E1876-09 Physical Testing Standards and Mechanical Testing Standards., in: Standard Test Method for Dynamic Young's Modulus, Shear Modulus, and Poisson's Ratio by Impulse Excitation of Vibration., ASTM International, 2009.

[46] ASTM, C1421-10 Standard Test Methods for Determination of Fracture Toughness of Advanced Ceramics at Ambient Temperature, in: Standard Test Methods for Determination of Fracture Toughness of Advanced Ceramics at Ambient Temperature, ASTM International 2010, pp. 31.

[47] A.A. Griffith, The Phenomena of Rupture and Flow in Solids, Philosophical Transactions of the Royal Society of London. Series A, Containing Papers of a Mathematical or Physical Character, 221 (1921) 163-198.

[48] R.W. Davidge, A.G. Evans, The Strength of Ceramics, Materials Science and Engineering, 6 (1970) 281-298.

[49] J.K. MacKenzie, The elastic constants of a solid containing spherical holes, Proceedings of the Physical Society. Section B, 63 (1950) 2-11.

[50] W. Kreher, J. Ranachowski, F. Rejmund, Ultrasonic waves in porous ceramics with non spherical holes, Ultrasonics, 15 (1977) 70-74.

[51] I. Ahrens, Mineral Physics and Crystallography: A Handbook of Physical Constants, American Geophysical Union, Washington, 1995.

[52] J. Gong, Y. Chen, C. Li, Statistical analysis of fracture toughness of soda-lime glass determined by indentation, Journal of Non-Crystalline Solids, 279 (2001) 219-223.

[53] R. Davidge, Mechanical Behaviour of Ceramics, Cambridge University Press, Cambridge, 1979.

[54] J.E. Ritter, F.M. Mahoney, K. Jakus, Fracture Mechanics of Ceramics, Plenum, New York, 1986.

[55] B.R. Lawn, Fracture of Brittle Solids, Cambridge University Press, Cambridge, 1993.

[56] C. Leonelli, P. Veronesi, V. Cannillo, G.C. Pellicani, A.R. Boccaccini, Porcelainized stoneware as a composite material: identification of strengthening and toughening mechanisms, Tile Brick Int., 17 (2001) 238-306.

[57] G. George A, Fracture toughness of ceramics and ceramic composites, Ceramics International, 29 (2003) 777-784.

[58] M. Albakry, M. Guazzato, M.V. Swain, Influence of hot pressing on the microstructure and fracture toughness of two pressable dental glass–ceramics, Journal of Biomedical Materials Research Part B: Applied Biomaterials, 71B (2004) 99-107.

[59] T. Rouxel, J.-C. Sanglebœuf, The brittle to ductile transition in a soda–lime–silica glass, Journal of Non-Crystalline Solids, 271 (2000) 224-235.

[60] N. Soga, Elastic moduli and fracture toughness of glass, Journal of Non-Crystalline Solids, 73 (1985) 305-313.

[61] S.M. Wiederhorn, Fracture Surface Energy of Glass, Journal of the American Ceramic Society, 52 (1969) 99-105.

[62] T. Rajan, A technique for measuring stresses in small spatial regions using cube-corner indentation: Application to tempered glass plates, J Eur Ceram Soc, 27 (2007) 2407-2414.

[63] Y.M. Ito, M. Rosenblatt, L.Y. Cheng, F.F. Lange, A.G. Evans, Cracking in particulate composites due to thermalmechanical stress, International Journal of Fracture, 17 (1981) 483-491.

[64] V.R. Mastelaro, E.D. Zanotto, Residual stresses in a soda-lime-silica glass-ceramic, Journal of Non-Crystalline Solids, 194 (1996) 297-304.

[65] F.A. Gilabert, M. Dal Bó, V. Cantavella, E. Sánchez, Fracture Patterns of Quartz Particles in Glass Feldspar Matrix, Materials Letters, 72 (2012) 148-152.